JCTC Journal of Chemical Theory and Computation

How Well Can Kohn−Sham DFT Describe the $HO_2 + O_3$ Reaction?

Luís P. Viegas, Adriana Branco, and António J. C. Varandas*

Departamento de Química, Universidade de Coimbra, 3004-535 Coimbra, Portugal

Received June 29, 2010

Abstract: In a previous work (*J. Chem. Theory Comput.* **2010**, *6*, 412) we reported an ab initio investigation of the reaction between ozone and the hydroperoxyl radical. The studies on this atmospheric reaction are here continued with an evaluation of different exchange-correlation functionals (all rungs of "Jacob's ladder" of density functional approximations are represented) in Kohn−Sham DFT calculations. We focus on the comparison between the barrier heights of the oxygen- and hydrogen-abstraction mechanisms here calculated with the ones previously obtained at the CASPT2(11,11)/AV*T*Z level. The comparison is also extended to the remaining stationary points. Additionally, a relation between the fraction of exact exchange of one-parameter hybrid functionals and the imaginary frequency of a saddle point is developed, originating three new functionals that are also used in the present benchmark calculations.

1. Introduction

Density functional theory (DFT)[1] is nowadays one of the most (if not the most) used methods of performing electronic structure calculations in the ground state of atoms, molecules, and solids. Its success stems from the simplification of the Schrödinger equation through the Hohenberg−Kohn (HK) theorems[2] and also from the practical implementation of the self-consistent Kohn−Sham (KS) equations.[3] These look like (and scale like) the Hartree−Fock equations, where the several terms that make up the ground-state energy (which HK proved to be a functional of the electron density, $E_0[\rho]$) can be calculated exactly except one, corresponding to a small fraction of the total energy and named exchange-correlation (xc) energy functional, $E_{xc}[\rho]$, which is unknown. KS-DFT is therefore exact in principle, while in practice $E_{xc}[\rho]$ must be approximated, thus being the main source of error in the theory. Such approximate functionals are often constructed[4] by constraint satisfaction (nonempirical functionals) or by fitting them to experimental and/or ab initio data (semiempirical functionals). It is believed that increasing the number of satisfied constraints is a step toward the exact and universal functional, but while this approach seems theoretically attractive, its progress has shown to be somewhat slow.[5] On the other hand, semiempirical functionals rapidly achieved widespread success, particularly through the popular B3LYP functional.[6] The semiempirical approach has the advantage of making accurate predictions for systems which belong (or are similar) to the training set, but it carries two main problems: one is the possible failure for systems outside the training set, and the other is that the functionals sometimes do not respect some of the known exact constraints. However, their low computational cost together with a huge predictive character for systems that cannot be correctly described by nonempirical functionals explains the great success of the semiempirical approach.

While in ab initio theory one knows exactly how to proceed to improve the quality of the results, in KS-DFT this is not so obvious and straightforward. One way to hierarchize and develop improved exchange-correlation functionals is by adding to them increasingly complex ingredients, therefore creating the possibility of satisfying more constraints. This is the basic philosophy behind the "Jacob's ladder"[5,7] of density functional approximations to the exchange-correlation energy, where functionals (nonempirical or semiempirical) are assigned to different rungs of the ladder, according to the complexity of their ingredients. As one naturally expects, on going up the ladder, accuracy and computational cost will generally increase. The first rung is the local spin density approximation (LSDA),[3] often referred to as the "mother of all approximations".[7] It uses as ingredients the spin densities $\rho_\alpha(\mathbf{r})$ and $\rho_\beta(\mathbf{r})$ and is by construction exact for uniform densities or densities that vary

* Corresponding author e-mail: varandas@qtvs1.qui.uc.pt.

10.1021/ct100364x
Published on Web 08/19/2010

very slowly over space. Many electronic systems do not respect these conditions (e.g., atoms and molecules), making LSDA more useful in solids. However, despite overestimating atomization and binding energies, LSDA gives good results in predicting properties like molecular geometries and vibrational frequencies,[8−11] being a useful structural tool except for thermochemistry.[12] The second rung is the generalized gradient approximation (GGA) which introduces the density gradients $\nabla\rho_\alpha(\mathbf{r})$ and $\nabla\rho_\beta(\mathbf{r})$ as additional ingredients. GGAs show a good improvement for thermochemistry[13,14] relative to LSDA. The third rung is the meta-generalized gradient approximation (meta-GGA), with $\nabla^2\rho_\alpha(\mathbf{r})$ and $\nabla^2\rho_\beta(\mathbf{r})$ being additional ingredients or, more commonly, the Kohn−Sham orbital kinetic energy densities $\tau_\alpha(\mathbf{r})$ and $\tau_\beta(\mathbf{r})$. The meta-GGAs mainly improve atomization energies[7,15] while keeping computational cost similar to the previous rungs.

The fourth rung is called hyper-GGA and employs the exact exchange (Hartree−Fock-like) energy density as an ingredient. These functionals are based on the adiabatic connection method (ACM)[12,16−18] and are also called hybrid functionals due to mixing of a fraction (a_0) of the exact exchange with GGA or meta-GGA exchange. The first hybrids were introduced by Becke,[19,20] and as many others that followed, they use a_0 as a constant (global hybrids), most often fitted to reproduce training sets and sporadically calculated theoretically.[19,21] However, besides not being system independent, a_0 is also not geometry independent for a given species,[22,23] a fact that led to the so-called local hybrids,[24−29] where $a_0(\mathbf{r})$ is a function of the coordinate space, mixing exact and DFT energy densities at each point in space. Hybrid functionals turned out to be a huge success in chemistry because of the great improvement over previous rungs in thermochemical calculations, particularly in calculating barrier heights, where exchange-correlation functionals are known to exhibit problems[30] (namely, by underestimating transition-state energies[31,32]). Such problems are known to be caused in part by the self-interaction error (SIE)[1,33] that becomes particularly important in nonequilibrium structures with stretched bonds.[34] Thus, they are a consequence of not including corrections[34,35] to the SIE in the approximate exchange-correlation functionals; the use of exact exchange will then be expected to reduce the SIE in KS-DFT calculations. The fifth and final rung of the ladder utilizes not only the occupied KS orbitals but also the unoccupied ones.[5] A special case of fifth-rung functionals are the double hybrids,[36] as they mix wave function methods with hybrid DFT ones. Typically, in a double-hybrid calculation, the KS orbitals and eigenvalues resulting from the self-consistent run are subsequently used in a MP2-like calculation of the correlation energy, which replaces some of the GGA or meta-GGA correlation.

The atmospherically important $HO_2 + O_3$ reaction[37−42] has been the subject of recent theoretical investigations,[43−46] where extensive ab initio calculations were performed in order to clarify its mechanism. Special emphasis was given to the saddle points that represent the attack of the hydroperoxyl radical to ozone from the O and H sides (**SP$_1$** and **SP$_4$** of ref 46, respectively), since these are the critical regions of the potential-energy surface (PES) that determine the dynamics of the reaction. Our goal with the present study is a fundamental one, and it is reflected in the article's title. We will answer the posed question by assessing the quality of several exchange-correlation functionals (belonging to different rungs of the "Jacob's ladder") in the description of the reaction mechanism. Such a methodology has been suggested in ref 47, where it is stated "Users should also report results on several different rungs, where possible, both as a check on consistency and as a guidance for functional developers." Again, our focus will be on calculation of the **SP$_1$** and **SP$_4$** barrier heights, with the best performing functionals being then used to study and compare the whole reaction mechanism here obtained with the one calculated and graphically represented in Scheme 1 of ref 46. Thus, the KS-DFT results will be compared to the ones calculated at the CASPT2(11,11)/AV*TZ*//CASSCF(11,11)/6-311++G(2df,2p) level of theory, which are probably the most reliable ab initio results reported thus far in the literature for the description of all stationary points of the $HO_5(^2A)$ PES, although multireference perturbation theory (MRPT) may not be free from problems.[48−52] Recall that the title reaction is a challenging one to theoretical methods,[53] since some of the regions of the PES show a high multireference character.[46] In addition, knowing that KS-DFT is sometimes problematic in describing saddle points makes it an interesting reaction for the benchmarking of KS-DFT. Finding a functional suitable for electronic calculations in the $HO_5(^2A)$ PES would be extremely useful in the study of the $HO_2 + O_3$ reaction, since the computational cost associated with KS-DFT is much lower than multireference perturbation theory, thus allowing an extensive mapping of the PES at the regions of interest.

The structure of the paper is as follows. In Computational Methods, the basic theory and technical details behind the calculations are described, whereas the next section reports the Results and Discussion. The conclusions are gathered in the last section.

2. Computational Methods

All calculations have been performed with the GAMESS[54] and ORCA[55] packages. The GAMESS code was used for all KS-DFT optimizations employing the M06 family of exchange-correlation functionals and also for all intrinsic reaction coordinate (IRC) calculations, while ORCA was used in the remaining calculations. While using both computer codes, a vibrational analysis of the harmonic vibrational frequencies was performed after each geometry optimization to confirm the nature of the stationary points. The MacMolPlt[56] graphical user interface was used for visualization of the different geometric and electronic features of the PES.

The following DFT functionals, ranked according to the "Jacob's ladder" of Perdew, have been considered in this work: first rung, LSDA;[3] second rung, BLYP[57,58] and PBE;[59] third rung, TPSS;[15] fourth rung (hybrid GGAs), B3LYP,[6] PBEh,[60,61] and BH&HLYP;[19,57,58] fourth rung (hybrid meta-

GGAs), M06,[62] M06-2X,[62] and M06-HF;[63] fifth rung, B2PLYP[64] and B2GP-PLYP.[65]

The following basis sets were used: 6-311++G(2df,2p), 6-311++G(2df,2pd), and aug-cc-pV*X*Z (*X* = *D*,*T* or simply AV*X*Z). Geometry optimizations were performed with the 6-311++G(2df,2p) basis set to allow a direct comparison between the geometrical parameters calculated here and in our previous study.[46] However, this basis set is not available in the ORCA package, and therefore, while using this code, we adopted the 6-311++G(2df,2pd) basis instead, which only adds 5 contracted basis functions in a calculation on the $HO_5(^2A)$ PES. We expect no significant changes with such a small difference between both basis sets. The energetic parameters, such as relative energies (with special emphasis on barrier heights), relaxation energies, and basis set superposition errors (BSSE), were calculated with Dunning basis sets, since the single-point energies of ref 46 were obtained with the AV*T*Z basis set.

Dispersion corrections to the DFT energies (DFT-D) were also included in the calculations. These are available in GAMESS and ORCA with Grimme's formulation,[66,67] and we performed a separate set of calculations by adding this correction to the BLYP, PBE, TPSS, B3LYP, and B2PLYP exchange-correlation functionals. The details and testing of this method can be found in the original publications[66,67] and also in some recent papers.[68−76] We should stress that no saddle points were found with TPSS-D, and therefore, no results with this functional will be shown.

All barrier heights (except the ones involving the M06 family of functionals) were calculated with BSSE corrections according to the counterpoise (CP) scheme proposed by Boys and Bernardi.[77] The relative energies were obtained by taking into account the geometric modifications of the fragments upon formation of the saddle points[78,79]

$$\Delta E^{CP} = E_{SP}^{opt} - \sum_{m=1}^{N} E_m^{opt} + \sum_{m=1}^{N} (E_m^{frz} - E_m^{frz,*}) \qquad (1)$$

where E_{SP}^{opt} is the optimized energy of the saddle point, the E_m's are the energies of the monomers (in this case we have two monomers, O_3 and HO_2, and so $N = 2$). The superscript "opt" denotes the individually optimized monomers, and "frz" refers to the monomers frozen in their saddle-point geometries. The asterisk (*) indicates a calculation with ghost orbitals. From these quantities useful information can be extracted, such as the BSSE itself (third term in the rhs of eq 1, which is expected to become smaller with increasing size of the basis set and to approach zero when the complete basis set (CBS) limit is reached[78]), and the relaxation energy of each monomer, given by $E_m^{frz} - E_m^{opt}$, which gives us an indication of how much the geometry of one monomer changes until it reaches its saddle-point geometry. Equation 1 could not be applied to the M06 functionals, since GAMESS does not support BSSE runs with KS-DFT calculations. Instead, and while using GAMESS, we adopted the strategy used before, by calculating the reactants as a supermolecule with the fragments separated by 150 Å, not including CP corrections. A further remark to note is that eq 1 and CP are not free from criticism, particularly for transition states (and other topographical features) that are at regions far from the separated reactants, thus making unclear what kind of correction is provided by considering the separate reactants at their geometries in the transition state (suffice to note that interacting fragments are not rigid blocks and that CP often overestimates the BSSE). Therefore, the recommendable approach would be CBS extrapolation.[80,81] However, in the absence of CBS extrapolation schemes for the various components of the KS-DFT energy, CP will be employed here for necessity.

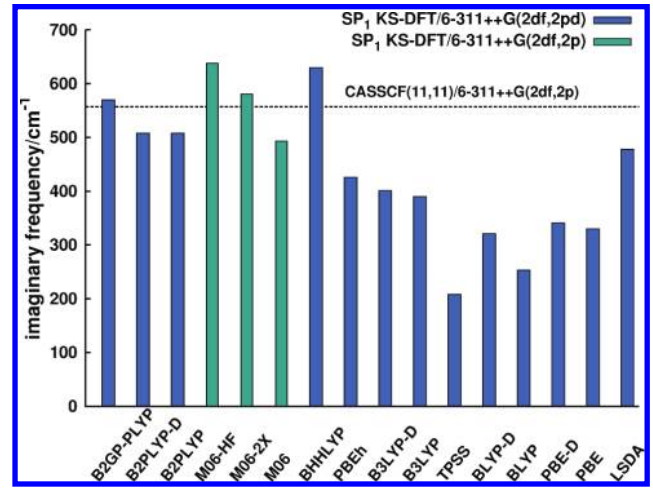

Figure 1. Comparison between the **SP$_1$** imaginary frequency calculated at the CASSCF(11,11)/6-311++G(2df,2p) level (dashed line) and at the KS-DFT level with two different basis sets and different exchange-correlation functionals.

In addition, and because the B2GP-PLYP results were included at the last minute with the most recent ORCA version (2.7 revision 0), we stress that all energetic parameters calculated with this functional and with the AV*T*Z basis set were in fact obtained at the B2GP-PLYP/AV*T*Z//B2GP-PLYP/AV*D*Z level, i.e., we did not perform optimizations with the AV*T*Z basis set in order to save computational time. Judging from previous calculations during the course of this work, the associated error with this approach should be less than 0.1 kcal mol^{-1}.

3. Results and Discussion

3.1. Saddle-Point Structures. We begin by comparing the imaginary frequencies of **SP$_1$** and **SP$_4$** obtained here with the ones obtained in ref 46. This can be seen in Figures 1 (**SP$_1$**) and 2 (**SP$_4$**), with the color indicating different basis sets. We also distributed the exchange functionals in the *X* axis according to their rank in the "Jacob's ladder", starting with LSDA (first rung) on the far right and ending with B2GP-PLYP (fifth rung) on the far left. In Figure 1, we can see a correlation between the rung to which each functional belongs and the quality of the calculated imaginary frequency. The exception is LSDA, which achieves a very good result, despite being the simplest functional in the set, and TPSS, which is the worse performing functional for such an imaginary frequency. The inclusion of dispersion corrections has also shown to improve the results, especially with BLYP, where an increase of 68 cm^{-1} is observed. Note also that B3LYP and PBEh performed quite poorly, despite the fact

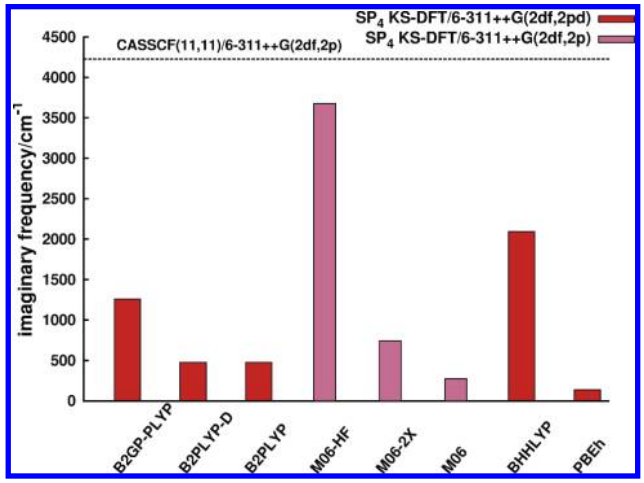

Figure 2. Comparison between the **SP$_4$** imaginary frequency calculated at the CASSCF(11,11)/6-311++G(2df,2p) level (dashed line) and KS-DFT level with two different basis sets and different exchange-correlation functionals.

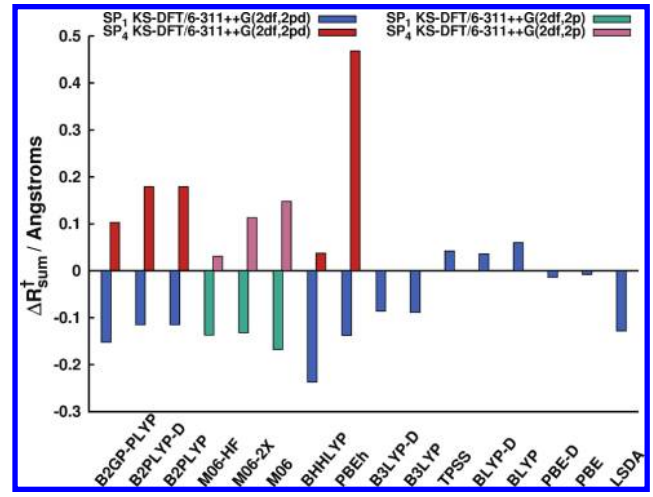

Figure 3. Comparison between the **SP$_1$** and **SP$_4$** perpendicular looseness calculated at the CASSCF(11,11)/6-311++G(2df,2p) level and KS-DFT level with two different basis sets and different exchange-correlation functionals (see text and eqs 2 and 3 for more details).

that they are fourth-rung functionals. This is most likely caused by their low percentage of exact exchange (20% and 25%, respectively).

Figure 2 shows a drastic reduction in the number of exchange functionals. This is because we were not able to optimize **SP$_4$** using functionals without exact exchange (first three rungs). Another interesting result is that **SP$_4$** could not be optimized with the popular B3LYP functional. In fact, the best result seen in Figure 2 is obtained with M06-HF, which incorporates 100% of exact exchange, followed by BH&HLYP with 50% of exact exchange and also B2GP-PLYP. The remaining imaginary frequencies show a huge disagreement with the CASSCF result, with no correlation between the functional's rung and the quality of its imaginary frequency. However, the role of the percentage of exact exchange reflects the crucial importance of the SIE in this saddle point, a common situation in hydrogen-abstraction mechanisms.[82−88] In this particular case, in which a hydrogen atom is transferred to ozone, we are in the presence of an odd-electron problem (three electrons in this case), which is known to be seriously plagued with SIE (see refs 86−88 and references therein). It is therefore natural that functionals with a higher percentage of exact exchange give better results since they "need" this contribution to cancel out the SIE originating in the Coulomb electron−electron interaction. This is also the case with the B2PLYP functional (53% of exact exchange), which has a lower percentage of exact exchange than double hybrids specifically parametrized for the calculation of barrier heights,[65,89] like B2GP-PLYP.

We also wanted to assess the quality of the saddle-point structures, so for each geometry we calculated its perpendicular looseness,[90] defined by

$$R^{\dagger}_{\mathrm{sum}} = R^{\dagger}(\text{breaking bond}) + R^{\dagger}(\text{forming bond}) \qquad (2)$$

and compared it with the ab initio value by means of the equation

$$\Delta R^{\dagger}_{\mathrm{sum}} = R^{\dagger}_{\mathrm{sum}}[\text{KS-DFT}] - R^{\dagger}_{\mathrm{sum}}[\text{ab initio}] \qquad (3)$$

with the ab initio calculations performed at the CASSCF-(11,11)/6-311++G(2df,2p) level.[46] The perpendicular looseness given by eq 2 "is a measure of the looseness of the structure in a direction perpendicular to the reaction coordinate".[90] It also gives us a rough measure of the quality of the calculated geometry, especially in the important region of the saddle-point structure, where one bond is broken and another one is formed. The results can be seen in Figure 3. Interestingly, for **SP$_1$**, the better (as before, by better we mean closest to the ab initio values) results are obtained with second- and third-rung functionals, being followed by B3LYP. This is also a known consequence of the presence of exact exchange; the molecular geometries are frequently better for functionals without it.[62,84] The majority of these saddle points is tighter than the CASSCF structures. As for **SP$_4$**, the best results are again obtained with BH&HLYP and M06-HF, with all of the structures being looser than the ab initio calculations. A particular bad result is obtained with PBEh, with its saddle point having a perpendicular looseness of almost 0.5 Å. In this particular case, the PBEh forming bond is ∼0.7 Å larger than the CASSCF forming bong, being the main source of error and clearly indicating a poor quality structure.

3.2. Barrier Heights. Figure 4 shows a graphical comparison between the KS-DFT and ab initio barrier heights; a numerical, more detailed, comparison is provided later. The **SP$_1$** barrier height calculated with the LSDA functional (− 11.72 kcal mol^{-1}) is not included in the figure in order to facilitate the visualization of the remaining barrier heights. For this saddle point the best barrier heights are the ones calculated with some of the highest rung functionals, namely, B2GP-PLYP and M06-HF. The widely used B3LYP functional shows disappointing results concerning barrier heights, but this is not surprising as it is well known that this functional often underestimates barrier heights due to the lack of exact exchange. A good example is given in ref 91. The inexistence of exact exchange can also be seen to

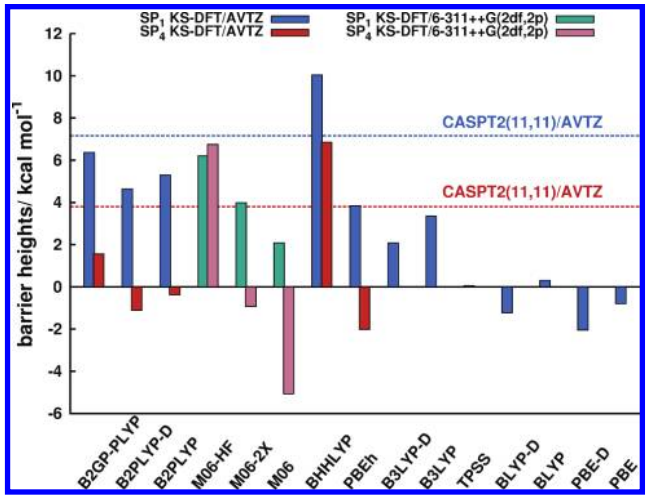

Figure 4. Comparison between the **SP_1** and **SP_4** barrier heights calculated at the CASPT2(11,11)/AV*T*Z level (**SP_1**, blue dashed line; **SP_4**, red dashed line) and KS-DFT level with two different basis sets and different exchange-correlation functionals.

dramatically affect the results obtained with functionals from the three lowest rungs.

The best functionals in calculating the barrier heights of **SP_4** are again (as it happened for the imaginary frequencies and perpendicular looseness) B2GP-PLYP, M06-HF, and BH&HLYP. However, M06-HF calculates an **SP_4** barrier higher than the **SP_1** one, contrary to experimental and ab initio results. In the case of BH&HLYP the difference between the **SP_1** and **SP_4** barriers (~3 kcal mol^{-1}) is consistent with the CASPT2(11,11)/AV*T*Z results. The remaining functionals do a very poor job in describing the **SP_4** barrier height, being energetically below the reactants. Note that PBEh (25% of exact exchange) has the second worse barrier height and shows the worse results for the imaginary frequency and perpendicular looseness. This is again explained by the large SIE present in transition states of chemical reactions, particularly hydrogen abstractions involving ozone.[86,87] The barrier heights of transition states calculated with KS-DFT are typically too low, which might be an indication that the BH&HLYP functional carries an excess of exact exchange for this specific reaction, since both barrier heights are well above the CASPT2 results.

In Tables 1 and 2 we present the barrier heights, BSSE, and relaxation energies calculated for **SP_1** and **SP_4** with the different exchange-correlation functionals and using the AV*D*Z and AV*T*Z basis sets, respectively. For reasons mentioned before, the numerical results concerning the M06 functionals are not included in these tables but will appear in a subsequent section. With the exception of the LSDA functional, all barrier heights of Table 2 were used in Figure 4. Note that by subtracting the BSSE (third column of Tables 1 and 2) from ΔE^{CP} in the second column one obtains the CP-free barrier heights. Concerning the BSSE, some comments should be made at this point. First, one observes the expected rapid decrease of the BSSE as the basis set size increases.[80,92] Excluding the double hybrids, all functionals show a BSSE below 0.4 kcal mol^{-1} with the AV*T*Z basis set, which is quite an acceptable result with this moderate size basis set. Now we turn to the double-hybrids BSSE results. Clearly, the BSSE is now higher than before, a result that can be rationalized by acknowledging that these functionals perform an MP2-type calculation, and these are known to converge rather unsystematically to the CBS limit.[93] As for the relaxation energies, one observes different behaviors in O_3 and HO_2. The **O_3/SP_1** relaxation energies tend to decrease with increasing size of the basis set (except for B2GP-PLYP and BLYP-D), while for **SP_4** this tendency is reversed, with PBEh being the only functional for which

Table 1. Energetic Parameters Available by Computing the Barrier Heights Using Eq 1[a]

method/SP	ΔE^{CP}	BSSE	O_3 relaxation	HO_2 relaxation
CASPT2(11,11)/SP_1	**7.160**			
B2GP-PLYP/SP_1	7.403	1.900	1.720	0.038
B2PLYP-D/SP_1	5.333	1.488	1.489	0.011
B2PLYP/SP_1	6.019	1.488	1.492	0.011
BH&HLYP/SP_1	10.609	0.901	1.928	0.184
PBEh/SP_1	4.112	0.767	1.517	0.008
B3LYP-D/SP_1	2.343	0.603	1.671	0.011
B3LYP/SP_1	3.563	0.535	1.647	0.005
TPSS/SP_1	−0.309	0.475	1.575	0.069
BLYP-D/SP_1	−1.384	0.309	1.885	0.052
BLYP/SP_1	0.379	0.421	1.592	0.016
PBE-D/SP_1	−2.017	0.497	1.907	0.080
PBE/SP_1	−0.907	0.469	1.859	0.083
LSDA/SP_1	−11.829	0.587	3.101	1.478
CASPT2(11,11)/SP_4	**3.810**			
B2GP-PLYP/SP_4	2.077	1.653	0.383	2.952
B2PLYP-D/SP_4	−0.867	1.242	0.392	1.384
B2PLYP/SP_4	−0.128	1.240	0.393	1.385
BH&HLYP/SP_4	6.751	0.790	0.600	5.953
PBEh/SP_4	−2.029	0.634	0.079	0.140

[a] The definition of BSSE and relaxation energies are given at the end of section 2. The energies are given in kcal mol^{-1}, and all calculations were performed with the AV*D*Z basis set. The CASPT2/AV*T*Z results were obtained from ref 46.

Table 2. Energetic Parameters Available by Computing the Barrier Heights Using Eq 1[a]

method/SP	ΔE^{CP}	BSSE	O_3 relaxation	HO_2 relaxation
CASPT2(11,11)/SP_1	**7.160**			
B2GP-PLYP/SP_1	6.370	1.107	2.078	0.088
B2PLYP-D/SP_1	4.644	0.825	1.348	0.012
B2PLYP/SP_1	5.309	0.825	1.351	0.012
BH&HLYP/SP_1	10.046	0.301	1.891	0.194
PBEh/SP_1	3.844	0.264	1.393	0.009
B3LYP-D/SP_1	2.093	0.182	1.513	0.009
B3LYP/SP_1	3.360	0.195	1.530	0.006
TPSS/SP_1	0.069	0.310	1.121	0.017
BLYP-D/SP_1	−1.226	0.268	1.964	0.053
BLYP/SP_1	0.303	0.098	1.343	0.019
PBE-D/SP_1	−2.038	0.133	1.657	0.069
PBE/SP_1	−0.792	0.248	1.597	0.064
LSDA/SP_1	−11.720	0.355	2.940	1.521
CASPT2(11,11)/SP_4	**3.810**			
B2GP-PLYP/SP_4	1.558	1.099	0.443	3.000
B2PLYP-D/SP_4	−1.113	0.810	0.416	1.585
B2PLYP/SP_4	−0.379	0.810	0.417	1.586
BH&HLYP/SP_4	6.860	0.275	0.649	6.304
PBEh/SP_4	−2.024	0.184	0.053	0.104

[a] The definition of BSSE and relaxation energies are given at the end of section 2. The energies are given in kcal mol^{-1}, and all calculations were performed with the AV*T*Z basis set. The CASPT2/AV*T*Z results were obtained from ref 46.

its relaxation energy diminishes. The HO_2 relaxation energies generally increase with increasing size of the basis set, except for B3LYP-D, TPSS, PBE(-D) (**SP$_1$**), and PBEh (**SP$_4$**). These relaxation energies indirectly tell us what happens in each reaction channel when going from reactants to these two different saddle points in the PES. In the oxygen-abstraction channel (**SP$_1$**) it is clear that the O_3 fragment suffers more drastic geometry changes than HO_2 because the ozone relaxation energy is always considerably larger than the hydroperoxyl one. This was likely to be observed, since one of the bonds in ozone is broken in this channel.[43,45,46] A similar analysis can be made to the hydrogen-abstraction channel (**SP$_4$**), where higher relaxation energies are now observed for the hydroperoxyl radical. These are consistent with the knowledge that in this reaction channel the OH bond is broken and that the O−O bond becomes smaller in the saddle-point geometry.[45,46] Because B2GP-PLYP and BH&HLYP give the best barrier heights for **SP$_4$** in Tables 1 and 2, one should pay particular attention to the HO_2 relaxation energies; they are in fact higher than the other three relaxation energies for this fragment. The information obtained from analyzing the relaxation energies might be useful in the future if one wants to map the PES in the region of the saddle points.

3.3. Improving One-Parameter Hybrids. In the previous two subsections we have seen that exchange-correlation functionals studied in this work have generally shown great difficulties in describing several aspects of **SP$_1$** and **SP$_4$**, with the latter being most problematic. By examining some relations between results obtained up to this point (imaginary frequencies, perpendicular looseness, and barrier heights) and also recognizing the tight relation between the quality of barrier heights and the fraction of exact exchange in KS-DFT, we decided to investigate further some of the involved connections. An investigation concerning the imaginary frequency seemed the most obvious choice, since it is known that its magnitude is directly associated with the height of the barriers.[85,94] A good description of the imaginary frequency ensures that the saddle point has the correct topology, which is a step toward obtaining a better barrier height. Since we also know that exact exchange has a major role in the calculation of barrier heights, we were compelled to study the relation between the percentage of exact exchange present in a functional and a saddle point's imaginary frequency. For simplicity, only one-parameter hybrids are investigated with an exchange-correlation expression of the type

$$E_{xc} = a_0 E_x^{exact} + (1 - a_0)E_x^{DFT} + E_c^{DFT} \qquad (4)$$

Our procedure was to vary the fraction of exact exchange [much in the spirit of the specific reaction parameter (SRP) method of ref 95; see also ref 96], a_0 in eq 4, and observe the behavior of the imaginary frequency. This can be done easily in ORCA, where there is the possibility of choosing the building blocks in an exchange-correlation functional. We did this by using three different forms of eq 4. The first one has E_x^{DFT} = B88 and E_c^{DFT} = LYP (with $a_0 = 0.5$ one gets BH&HLYP), the second one has DFT = PBE (with $a_0 = 0.25$ one gets PBEh), and the third one has DFT = TPSS (with $a_0 = 0.10$ one gets TPSSh,[97] a hybrid meta-GGA functional). Recall that the ab initio imaginary frequency was obtained with the 6-311++G(2df,2p) basis set, so in principle we should use the closest basis set possible (in this case, the 6-311++G(2df,2pd)). However, because the differences in the imaginary frequencies using AV*DZ* and 6-311++G(2df,2pd) are very small (most often around 3 or 4 cm^{-1}), we performed the saddle-point optimizations with the AV*DZ* basis set, thus saving considerable computational time while not compromising the main conclusions drawn from this part of our study. a_0 was varied from 0.2 to 0.8, in intervals of 0.1 with each of the three forms of eq 4, thus covering a large fraction of exact exchange. The resulting set of points is represented in Figure 5, where a strong resemblance between the three sets of points can be observed, especially the ones for which E_x^{DFT} = B88 and TPSS. Visual inspection of Figure 5 reveals that in order to match the ab initio imaginary frequency of $557i$ cm^{-1}, one needs approximately 40% of exact exchange. The next step was to solve a system of linear equations in order to find the coefficients for the expression that calculates the imaginary frequency ($\omega^{\dagger}$) of **SP$_1$** as a function of the percentage of exact exchange ($X = 100a_0$)

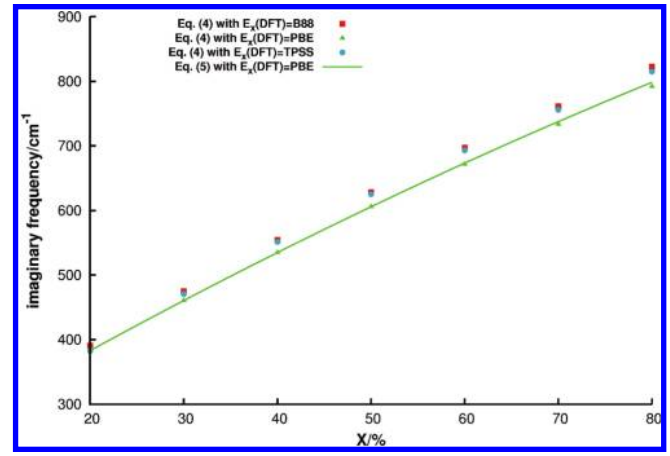

Figure 5. Imaginary frequencies of **SP$_1$** (squares, triangles, and circles) calculated at the KS-DFT/AV*DZ* level using three different exchange functionals of the form of eq 4 as a function of the percentage of exact exchange ($X = 100a_0$). Also represented in this figure is the curve obtained using eq 5 with E_x^{DFT} = PBE with parameters given in Table 3.

$$\omega^{\dagger} = aX^2 + bX + c \qquad (5)$$

The values of X used to solve the system of equations were naturally chosen as $X = 30$, 40, and 50, because they are the ones closest to our approximate prediction of X. Figure 5 shows the calculated curve based on eq 5 for which E_x^{DFT} = PBE. We then used the three calculated curves given by eq 5 to extract X for which $\omega^{\dagger} = 557i$ cm^{-1}. The relevant data is collected in Table 3. Note that opting for a fit to the calculated points, the values of X differ from the ones given in Table 3 at most by 0.07%. The values obtained for X define three new exchange-correlation functionals: BLYP-VBV, PBE-VBV, and TPSS-VBV (the names were given to facilitate the reading of the remaining of this paper). Interestingly, our calculated values of X are very similar to

Table 3. Parameters Determined for Eq 5[a]

exchange functional	a/cm^{-1}	b/cm^{-1}	c/cm^{-1}	interpolated X/%
B88	−0.02560	9.7100	206.71	40.4
PBE	−0.01665	8.5895	217.83	43.1
TPSS	−0.03505	10.5255	186.35	40.7

[a] The imaginary frequencies were obtained by saddle-point optimizations with the AV*DZ* basis set using three different exchange-correlation functionals of the form of eq 4, with each different exchange functional used being shown in the first column. The last column gives the interpolated value of X for which $\omega^{\dagger} = 557i$ cm^{-1}. The new values of X define the three new functionals used in this work.

the ones used in one-parameter hybrids specially designed for calculating accurate barrier heights, such as MPW1K[98] (hybrid GGA) and BB1K[99] (hybrid meta-GGA) which incorporate 42.8% and 42% of exact exchange, respectively. Note that ORCA has the exchange and correlation functionals necessary to build the one-parameter hybrid mPW1PW[100] ($a_0 = 0.25$) and therefore MPW1K ($a_0 = 0.428$), but unfortunately we encountered severe numerical difficulties while using this particular implementation of the mPW exchange functional.[100] For this reason, we were forced to stop the calculations with this hybrid. We further note that the exchange and correlation functionals that make up PBE-VBV and MPW1K have a close similarity,[4] which leads us to believe that because of this and the identical fractions of exact exchange they should yield very similar results.

We also tested this approach with the **SP$_4$** imaginary frequencies, but the fraction of exact exchange needed to reproduce the ab initio imaginary frequency was very high, approximately 75%. This led to huge barrier heights, and therefore, we discarded the optimization of **SP$_4$** using the described procedure as a valid way to calculate optimum X values. There are several possible explanations for this. One is that the ab initio imaginary frequency is miscalculated. Another is that the three tested one-parameter hybrid functionals cannot correctly calculate this frequency in such a problematic region of the PES. Although we cannot discard the former, we believe that the latter hypothesis is the correct one, since the imaginary frequency obtained with M06-HF has an acceptable agreement with the ab initio value, thus suggesting that it is possible to have a functional that calculates reasonable imaginary frequencies and barrier heights for **SP$_4$**. Ideally, application of the above procedure separately to each saddle point would lead to the same fraction of exact exchange. However, because we believe (for reasons mentioned earlier) that not all such one-parameter hybrids may be able to mimic correctly (in the sense of matching the ab initio information) the imaginary frequency at **SP$_4$** with a moderately low value of X, we have chosen instead to employ the parameters resulting from the **SP$_1$** analysis to predict other regions of configuration space, **SP$_4$** included. Of course, one could always opt for a fit to the barrier heights or even to the difference between **SP$_1$** and **SP$_4$**. This was not the followed strategy for several reasons: (a) fits to barrier heights have been massively done in the literature; (b) it would be computationally much more expensive due to the basis set sizes and number of calculations needed to accurately perform such calculations; (c) the adopted strategy looked more interesting because of the fewer related publications that are available.

Table 4. Energetic Parameters of the New Functionals Defined in This Work[a]

method/SP	ΔE^{CP}	ΔE^{CP} + ZPE	BSSE	O_3 relaxation	HO_2 relaxation
CASPT2(11,11)/SP$_1$	**7.160**				
BLYP-VBV/SP$_1$	8.435	10.185	0.755	1.866	0.099
PBE-VBV/SP$_1$	8.307	10.147	1.033	1.645	0.069
TPSS-VBV/SP$_1$	8.808	10.628	1.119	1.749	0.105
CASPT2(11,11)/SP$_4$	**3.810**				
BLYP-VBV/SP$_4$	3.470	2.370	0.731	0.576	4.341
PBE-VBV/SP$_4$	2.680	1.830	0.957	0.455	3.775
TPSS-VBV/SP$_4$	4.126	2.996	0.979	0.490	4.596

[a] The barrier heights were computed using eq 1, and the definition of BSSE and the relaxation energies are given at the end of section 2. The energies are given in kcal mol^{-1}, and all calculations were performed with the AV*DZ* basis set, except for the CASPT2/AV*TZ* results, obtained from ref 46.

Table 5. Energetic Parameters of the New Functionals Defined in This Work[a]

method/SP	ΔE^{CP}	ΔE^{CP} + ZPE	BSSE	O_3 relaxation	HO_2 relaxation
CASPT2(11,11)/SP$_1$	**7.160**				
BLYP-VBV/SP$_1$	8.030	9.770	0.275	1.842	0.107
PBE-VBV/SP$_1$	7.822	9.622	0.303	1.586	0.080
TPSS-VBV/SP$_1$	8.453	10.253	0.370	1.721	0.127
CASPT2(11,11)/SP$_4$	**3.810**				
BLYP-VBV/SP$_4$	3.565	2.415	0.242	0.624	4.664
PBE-VBV/SP$_4$	2.852	1.842	0.317	0.501	4.118
TPSS-VBV/SP$_4$	4.466	3.186	0.393	0.565	5.033

[a] The barrier heights were computed using eq 1, and the definition of BSSE and the relaxation energies are given at the end of section 2. The energies are given in kcal mol^{-1}, and all calculations have been performed with the AV*TZ* basis set. The CASPT2/AV*TZ* results were obtained from ref 46.

Having determined the relation between X and $\omega^{\dagger}$, one is now faced with an obvious question: What will happen to the barrier heights when calculated with these three new functionals? To answer this question, we made new optimizations based on the BLYP-VBV, PBE-VBV, and TPSS-VBV functionals and recalculated the **SP$_1$** and **SP$_4$** barrier heights. These calculations were again performed with the AV*DZ* and AV*TZ* basis sets, like the ones presented in Tables 1 and 2. The new results can be seen in Tables 4 and 5 and also in Figure 6. As before, by subtracting the BSSE in the fourth column from ΔE^{CP} in the second one, one obtains the barrier heights without CP correction. The improvement of the barrier heights calculated with the new functionals can be easily acknowledged, especially for **SP$_4$**. Similar results are expected with the MPW1K and BB1K functionals because they are also one-parameter hybrids with a very similar fraction of exact exchange. Between the three new functionals, the best performance comes from BLYP-VBV and TPSS-VBV, depending on whether one is looking at the average error in the absolute barrier heights or at the error in the difference between **SP$_1$** and **SP$_4$**, respectively. The inclusion of the zero-point energies (ZPE) of the reactants and saddle points in the calculation of the barrier heights widens the gap between **SP$_1$** and **SP$_4$** even further, since it lowers **SP$_4$** and increases **SP$_1$**.

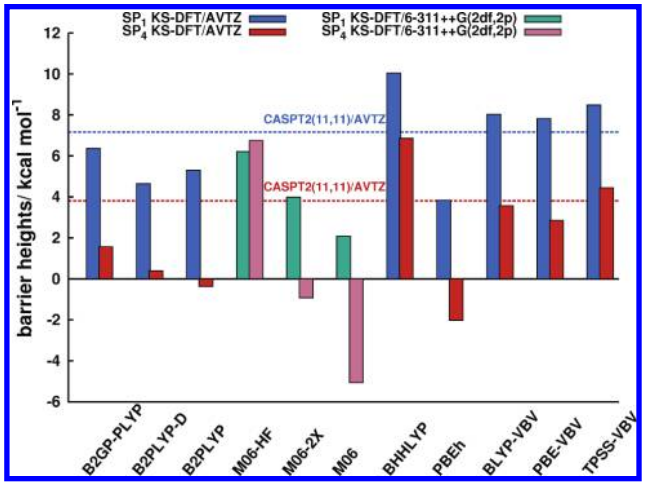

Figure 6. Comparison between the $\mathbf{SP_1}$ and $\mathbf{SP_4}$ barrier heights calculated at the CASPT2(11,11)/AV*T*Z level ($\mathbf{SP_1}$, blue dashed line; $\mathbf{SP_4}$, red dashed line) and KS-DFT level with two different basis sets and with all exchange-correlation functionals used in this work capable of optimizing both saddle points.

Table 6. Relative Energies, in kcal mol^{-1}, of the Different Stationary Points Along the IRC Path, Relative to the Reactants, Calculated with the 6-311++G(2df,2p) Basis Set[a]

method	MIN_1	MIN_2	MIN_3	SP_1	SP_2	SP_3	SP_4
CASPT2(11,11)	−3.50	−23.92	−35.06	7.16	−3.43	−20.88	3.81
M06-HF	−5.23	−16.53	−45.14	6.20		−14.18	6.75
M06−2X	−6.02		−43.89	3.99			−0.93
M06	−6.04		−38.16	2.09	−5.76		−5.07
BH&HLYP	−3.30		−38.53	9.72	−3.20		6.33
BLYP-VBV	−3.14		−39.12	7.74	−3.02		3.14
PBE-VBV	−3.53		−39.70	7.48			2.23
TPSS-VBV	−3.04		−38.03	7.95	−2.95		3.68

[a] The single-point CASPT2(11,11)/AV*T*Z energies are shown for comparison.

At this point, six exchange-correlation functionals stand out from the rest: B2GP-PLYP, M06-HF, BH&HLYP, BLYP-VBV, PBE-VBV, and TPSS-VBV.

3.4. IRC Calculations. Knowing which functionals calculate better both barrier heights, we proceed by evaluating their performance in the description of the IRC path. Do these functionals calculate the same number and type of stationary points along the reaction path as the previous[46] CASSCF(11,11)/6-311++G(2df,2p) calculations? How do the relative energies compare to the CASPT2 results? Since ORCA does not perform IRC calculations, B2GP-PLYP was excluded from the calculations. Additionally, we also performed IRC calculations with M06 and M06-2X. A locally modified version of GAMESS was used to calculate the IRC path of the reaction with BLYP-VBV, PBE-VBV, and TPSS-VBV. All calculations were carried out with the 6-311++G(2df,2p) basis set, without BSSE corrections, as explained in section 2, with the results being shown in Table 6.

The first thing that should be mentioned is the difference between the BH&HLYP results of Table 6 and the ones obtained in ref 46. The explanation is simple, as the BH&HLYP energies in our previous work were calculated as single-point energies for geometries optimized at the CASSCF(11,11)/6-311++G(2df,2p) level, while in Table 6 all energies concerning a specific functional are the result of geometry optimizations and IRC calculations with the same functional.

The IRC path calculated with the M06-HF functional is the one that resembles most the ab initio CASSCF calculations, since it is the only one that optimizes $\mathbf{MIN_2}$ and $\mathbf{SP_3}$. However, the relative energies between M06-HF and CASPT2 differ quite dramatically in some points. Additionally, and after many runs, the $\mathbf{SP_2}$ saddle point could not be optimized. In fact, this saddle point could not also be optimized with M06-2X and PBE-VBV, which means that these three functionals generate an extremely flat PES in this region. This problem was also addressed in ref 46. This saddle point connects two isomers with the same energy, $\mathbf{MIN_1}$; each of them has the HO_2 fragment tilted to one of the ozone extreme oxygen atoms, $\mathbf{MIN_{1L}}$ and $\mathbf{MIN_{1R}}$ (see Figure 3 of ref 44 and Figure 1 of ref 46). In the ab initio IRC calculations, $\mathbf{MIN_{1L}}$ is connected to $\mathbf{SP_1}$, while no minimum structure is associated with the IRC path in the direction of the reactants coming from $\mathbf{SP_4}$. In our KS-DFT calculations, things are slightly different. Except for M06-HF, which has $\mathbf{MIN_{1L}}$ associated with $\mathbf{SP_1}$ and $\mathbf{SP_4}$, the remaining functionals shown in Table 6 have $\mathbf{MIN_{1R}}$ associated with $\mathbf{SP_1}$ and $\mathbf{MIN_{1L}}$ associated with $\mathbf{SP_4}$.

Another interesting aspect of the KS-DFT calculations is related to the geometry of the HO_3 fragment in $\mathbf{MIN_3}$. Ab initio studies have shown that the equilibrium geometry of the hydrogen trioxy radical is strongly dependent on the theoretical method used (see ref 101 and references therein). Three minimum structures are known, one is *gauche*-HO_3,[102] with the hydrogen atom out of the plane formed by the three oxygen atoms, and the other two are the planar isomers *cis*- and *trans*-HO_3.[103] The HO_3 geometries in $\mathbf{MIN_3}$ obtained with the functionals of Table 6 also show this kind of dependence. BLYP-VBV and PBE-VBV calculate a *cis*-HO_3 structure and M06-HF a *cis*-like-HO_3 structure (one of the atoms is slightly off the plane). M06 and M06-2X calculate a *trans*-like-HO_3 structure, while BH&HLYP and TPSS-VBV originate a *gauche*-HO_3 structure. Table 7 shows the geometric parameters of HO_3 obtained experimentally[104] and calculated at different levels of theory. Besides the already mentioned differences in the dihedral angles ($D(O_1O_2O_3H)$, these defining the *cis*-, *trans*-, or *gauche*-type of structures), the largest differences are observed in the long O_2O_3 bond and in the O_2O_3H angle, consistent with recently reported theoretical work.[101,105,106]

Looking at the energetics of the stationary points, one can see that the new functionals, while improving the description of $\mathbf{SP_1}$ and $\mathbf{SP_4}$, still maintain a reasonable quality throughout the remaining structures. This can clearly be seen with BH&HLYP and BLYP-VBV, which differ only by the amount of exact exchange in each of them, 50% and 40.4%, respectively. This decrease of exact exchange has a large effect on $\mathbf{SP_1}$ (decrease of 1.98 kcal mol^{-1}) and $\mathbf{SP_4}$ (decrease of 3.19 kcal mol^{-1}) and a rather small effect on the remaining points, the largest being of 0.59 kcal mol^{-1} for $\mathbf{MIN_3}$. In fact, the KS-DFT energies of this minimum are always below the CASPT2 value by at least ∼3 kcal

Table 7. Comparison between the Geometric Parameters of HO_3 Obtained Experimentally[104] and Theoretically[a]

method	$d(O_1O_2)$	$D(O_2O_3)$	$d(O_3H)$	$A(O_1O_2O_3)$	$A(O_2O_3H)$	$D(O_1O_2O_3H)$
expt[104]	1.225	1.688	0.972	111.02	90.04	180.00
MRCI[105]	1.233	1.647	0.960	107.40	96.60	180.00
CASSCF(11,11)[46]	1.259	1.476	0.946	108.77	100.34	−99.91
M06-HF	1.250	1.397	0.969	111.41	101.99	−5.68
M06−2X	1.241	1.452	0.968	109.42	100.08	−154.23
M06	1.228	1.494	0.969	109.69	99.28	−172.46
BH&HLYP	1.251	1.424	0.958	111.04	101.97	−84.62
BLYP-VBV	1.250	1.439	0.966	111.96	101.48	0.00
PBE-VBV	1.239	1.412	0.963	111.91	101.57	0.00
TPSS-VBV	1.246	1.430	0.960	111.08	101.52	−86.14

[a] The MRCI geometry was calculated at the MRCI/6-311+G(d,p)//CASSCF(13,13) level[105] (*trans*- HO_3), while the remaining geometries concern the HO_3 fragment of **MIN$_3$** optimized at the CASSCF(11,11)[46] and KS-DFT level with the 6-311++G(2df,2p) basis set. Distances (*d*,*D*) are in Angstroms, and angles (*A*,*D*) are in degrees.

mol^{-1}, reaching a high error of ∼10 kcal mol^{-1} with M06-HF and M06-2X. Note also that the **SP$_1$** and **SP$_4$** barrier heights of Table 6 are slightly below the ones of Tables 4 and 5. This is mainly due to the fact that in Table 6 the relative energies were calculated assuming the reactants as a supermolecule, with the fragments separated by 150 Å, as carried out in ref 46, instead of using eq 1. In fact, if these barrier heights are recalculated with the three new functionals by performing single-point energy calculations with the AV*T*Z basis set, one obtains for **SP$_1$** and **SP$_4$**, respectively, 7.71 and 3.28 kcal mol^{-1} for BLYP-VBV, 7.49 and 2.50 kcal mol^{-1} for PBE-VBV, and 8.06 and 4.03 kcal mol^{-1} for TPSS-VBV, generally improving further the agreement with the CASPT2(11,11)/AV*T*Z results.

It recently came to our attention a publication concerning the integration grid errors of the M06 suite of functionals,[107] where it is concluded that the grid errors arise from integration errors in the exchange component of the energy. This becomes even more problematic for M06-HF, where the grid errors in predicting reaction energies in a set of 34 organic reactions are shown to go from −6.7 to 3.2 kcal mol^{-1}. Our computations with the GAMESS package were performed with its default grid (96 radial points and 288 angular points (96,288)), and so we performed a separate set of calculations with a larger grid, namely (200,1202), to check if there was any major error associated with our calculations. All absolute energies calculated with the larger grid were shifted positively by less than 1×10^{-4} E_h (∼0.06 kcal mol^{-1}) from the initial energies, a small error that essentially disappears when performing energy differences.

4. Conclusions

In this work we performed a KS-DFT computational benchmark study of the reaction between ozone and the hydroperoxyl radical, comparing the results with the ones resulting from our previous ab initio study.[46] Because of the nature of our investigation, we used exchange-correlation functionals from all rungs of the "Jacob's ladder" of density functional approximations in order to assess the performance of a wide range of functionals in describing this particular reaction. Our main concern was to evaluate the quality of the KS-DFT barrier heights of the oxygen- and hydrogen-abstraction mechanisms, since we are primarily interested in the dynamics of this reaction. The best functionals were subsequently used to calculate the remaining stationary points along the reaction coordinate and to compare the energetics with the CASPT2 calculations.

The barrier heights were shown to be improved using functionals incorporating exact exchange (fourth and fifth rungs of the ladder), as a consequence of the decrease of the SIE in the saddle-point geometries. However, in our first batch of calculations, none of the exchange-correlation functionals lead to good barrier heights for both saddle points, **SP$_1$** and **SP$_4$**. This difficulty is probably extendable in the study of reactions with such complex electronic structure features. We then proceeded by investigating the relation between the fraction of exact exchange in three one-parameter hybrids and the imaginary frequencies of the saddle points. By making the KS-DFT imaginary frequencies match the **SP$_1$** ab initio one, we obtained $X \approx 40\%$ for the three new functionals (BLYP-VBV, PBE-VBV, and TPSS-VBV), improving both barrier heights. This fraction of exact exchange is very similar to the one existing in functionals that were fitted to barrier heights and are very efficient in thermochemical kinetics.[98,99] For this reason, it is possible that these three new functionals are also generally suited for kinetics, but to confirm this hypothesis it would be necessary to test them against several databases. However, we stress that our focus is not on the new functionals but rather on the methodology followed to obtain them, as it allowed us to improve our KS-DFT results with a computationally fast and chemically driven procedure. The method also gave us some latitude in which exchange and correlation functionals to choose from when building the final functional. This happened to be quite useful, since our needs were not satisfied by any of the functionals defined in the quantum chemistry packages available in our group.

Finally, we would also like to point out that we recognize the subjectivity inherent to the choice of ab initio method to which the KS-DFT results should be compared to. For this reaction, considering its number of atoms and electronic structure details,[46] the CASPT2(11,11)/AV*T*Z//CASSCF-(11,11)/6-311++G(2df,2p) level of theory was pretty much the best that we could do with the available computational power at our disposal. This of course does not necessarily mean that those will be, henceforth, the best ab initio calculations available for this reaction. In fact, some studies reveal that MRPT is problematic,[48−50] while in other cases it shows a lower accuracy when compared to certain functionals,[51,52] even for single-reference systems. Some

caution should then be exercised when using MRPT results. For example, a plausible scenario (among many other possibilities) would be one in which the MPW1K functional (or, due to their similarity, PBE-VBV) could be the best one to reproduce the barrier heights calculated at some higher level of theory, say multireference configuration interaction calculations. Nevertheless, we think that this study shows a fairly reliable and fast alternative to perform electronic structure calculations for studying the $HO_2 + O_3$ reaction.

Acknowledgment. The authors acknowledge funding from Fundação para a Ciência e a Tecnologia, Portugal (contracts PTDC/QUI-QUI/099744/2008, PTDC/AAC-AMB/099737/2008, and SFRH/BPD/40807/2007).

References

(1) Parr, R. G.; Yang, W. *Density-Functional Theory Of Atoms and Molecules*; Oxford University Press: New York, 1989.

(2) Hohenberg, P.; Kohn, W. *Phys. Rev.* **1964**, *136*, B864.

(3) Kohn, W.; Sham, L. J. *Phys. Rev.* **1965**, *140*, A1133.

(4) Scuseria, G. E.; Staroverov, V. N. Progress in the development of exchange-correlation functionals. In *Theory and Applications of Computational Chemistry: The First Forty Years*; Dykstra, C. E., Frenking, G., Kim, K. S., Scuseria, G. E., Eds.; Elsevier: Amsterdam, 2005; p 669.

(5) Perdew, J. P.; Ruzsinszky, A.; Tao, J.; Staroverov, V. N.; Scuseria, G. E.; Csonka, G. I. *J. Chem. Phys.* **2005**, *123*, 062201.

(6) Stephens, P. J.; Devlin, F. J.; Chabalowski, C. F.; Frisch, M. J. *J. Phys. Chem.* **1994**, *98*, 11623.

(7) Perdew, J. P.; Schmidt, K. Jacob's ladder of density functional approximations for the exchange-correlation energy. In *Density Functional Theory and Its Application to Materials*; Van Doren, V., Van Alsenoy, C., Geerlings, P., Eds.; AIP: Melville, NY, 2001; p 1.

(8) Jones, R. O.; Gunnarsson, O. *Rev. Mod. Phys.* **1989**, *61*, 689.

(9) Delley, B. *J. Chem. Phys.* **1991**, *94*, 7245.

(10) Andzelm, J.; Wimmer, E. *J. Chem. Phys.* **1992**, *96*, 1280.

(11) Johnson, B. G.; Gill, P. M. W.; Pople, J. A. *J. Chem. Phys.* **1993**, *98*, 5612.

(12) Kohn, W.; Becke, A. D.; Parr, R. G. *J. Phys. Chem.* **1996**, *100*, 12974.

(13) Becke, A. D. *J. Chem. Phys.* **1992**, *96*, 2155.

(14) Becke, A. D. *J. Chem. Phys.* **1992**, *97*, 9173.

(15) Tao, J.; Perdew, J. P.; Staroverov, V. N.; Scuseria, G. E. *Phys. Rev. Lett.* **2003**, *91*, 146401.

(16) Harris, J.; Jones, R. O. *J. Phys. F* **1974**, *4*, 1170.

(17) Gunnarsson, O.; Lundqvist, B. I. *Phys. Rev. B* **1976**, *13*, 4274.

(18) Langreth, D. C.; Perdew, J. P. *Phys. Rev. B* **1977**, *15*, 2884.

(19) Becke, A. D. *J. Chem. Phys.* **1993**, *98*, 1372.

(20) Becke, A. D. *J. Chem. Phys.* **1993**, *98*, 5648.

(21) Perdew, J. P.; Ernzerhof, M.; Burke, K. *J. Chem. Phys.* **1996**, *105*, 9982.

(22) Gritsenko, O. V.; Van Leeuwen, R.; Baerends, E. J. *Int. J. Quantum Chem.* **1996**, *60*, 1375.

(23) Ernzerhof, M.; Perdew, J. P.; Burke, K. *Int. J. Quantum Chem.* **1997**, *64*, 285.

(24) Jaramillo, J.; Scuseria, G. E.; Ernzerhof, M. *J. Chem. Phys.* **2003**, *118*, 1068.

(25) Mori-Sánchez, P.; Cohen, A. J.; Yang, W. *J. Chem. Phys.* **2006**, *124*, 091102.

(26) Arbuznikov, A. V.; Kaupp, M. *Chem. Phys. Lett.* **2007**, *440*, 160.

(27) Perdew, J. P.; Ruzsinszky, A.; Csonka, G. I.; Vydrov, O. A.; Scuseria, G. E.; Staroverov, V. N.; Tao, J. *Phys. Rev. A* **2007**, *76*, 040501.

(28) Perdew, J. P.; Staroverov, V. N.; Tao, J.; Scuseria, G. E. *Phys. Rev. A* **2008**, *78*, 052513.

(29) Haunschild, R.; Scuseria, G. E. *J. Chem. Phys.* **2010**, *132*, 224106.

(30) Perdew, J. P.; Ernzerhof, M. Driving out the self-interaction error. In *Electronic Density Functional Theory: Recent Progress and New Directions*; Dobson, J. F., Vignale, G., Das, M. P., Eds.; Plenum: New York, 1998; p 31.

(31) Lynch, B. J.; Zhao, Y.; Truhlar, D. G. *J. Phys. Chem. A* **2003**, *107*, 1384.

(32) Zhao, Y.; Pu, J.; Lynch, B. J.; Truhlar, D. G. *Phys. Chem. Chem. Phys.* **2004**, *6*, 673.

(33) Levine, I. N. Ab initio and density-functional treatments of molecules. In *Quantum Chemistry*, 5th ed.; Prentice-Hall: New Jersey, 2000; p 581.

(34) Patchkovskii, S.; Ziegler, T. *J. Chem. Phys.* **2002**, *116*, 7806.

(35) Perdew, J. P.; Zunger, A. *Phys. Rev. B* **1981**, *23*, 5048.

(36) Zhao, Y.; Lynch, B. J.; Truhlar, D. G. *J. Phys. Chem. A* **2004**, *108*, 4786.

(37) Duewer, W. H.; Wuebbles, D. J.; Ellsaesser, H. W.; Chang, J. S. *J. Geophys. Res.* **1977**, *82*, 935.

(38) Crutzen, P. J.; Howard, C. J. *Pure Appl. Geophys.* **1978**, *116*, 497.

(39) Whitten, R. C.; Borucki, W. J.; Capone, L. A.; Turco, R. P. *Nature* **1978**, *275*, 523.

(40) Turco, R. P.; Whitten, R. C.; Poppoff, I. G.; Capone, L. A. *Nature* **1978**, *276*, 805.

(41) Wennberg, P. O.; et al. *Science* **1994**, *266*, 398.

(42) Monks, P. S. *Chem. Soc. Rev.* **2005**, *34*, 376.

(43) Varandas, A. J. C.; Zhang, L. *Chem. Phys. Lett.* **2004**, *385*, 409.

(44) Mansergas, A.; Anglada, J. M. *J. Phys. Chem. A* **2007**, *111*, 976.

(45) Xu, Z. F.; Lin, M. C. *Chem. Phys. Lett.* **2007**, *440*, 12.

(46) Viegas, L. P.; Varandas, A. J. C. *J. Chem. Theory Comput.* **2010**, *6*, 412.

(47) Perdew, J. P.; Ruzsinszky, A.; Constantin, L. A.; Sun, J.; Csonka, G. I. *J. Chem. Theory Comput.* **2009**, *5*, 902.

(48) Rode, M. F.; Werner, H.-J. *Theor. Chem. Acc.* **2005**, *114*, 309.

(49) Cramer, C. J.; Włoch, M.; Piecuch, P.; Puzzarini, C.; Gagliardi, L. *J. Phys. Chem. A* **2006**, *110*, 1991.

(50) Cramer, C. J.; Kinal, A.; Włoch, M.; Piecuch, P.; Gagliardi, L. *J. Phys. Chem. A* **2006**, *110*, 11557.

(51) Tishchenko, O.; Zhen, J.; Truhlar, D. G. **2008**, *4*, 1208.

(52) Zhen, J.; Zhao, Y.; Truhlar, D. G. **2009**, *5*, 808.

(53) Zhao, Y.; Tishchenko, O.; Gour, J. R.; Li, W.; Lutz, J. J.; Piecuch, P.; Truhlar, D. G. *J. Phys. Chem. A* **2009**, *113*, 5786.

(54) Schmidt, M. W.; Baldridge, K. K.; Boats, J. A.; Elbert, S. T.; Gorgon, M. S.; Jensen, J. H.; Koseki, S.; Matsunaga, N.; Nguyen, K. A.; Su, S.; Windus, T. L.; Dupuis, M.; Montgomery, J., Jr. *J. Comput. Chem.* **1993**, *14*, 1347.

(55) Neese, F. *ORCA - an ab initio, Density Functional and Semiempirical program package*, Version 2.6-35; University of Bonn, 2008.

(56) Bode, B. M.; Gordon, M. S. *J. Mol. Graphics Modell.* **1998**, *16*, 133.

(57) Becke, A. D. *Phys. Rev. A* **1988**, *38*, 3098.

(58) Lee, C.; Yang, W.; Parr, R. G. *Phys. Rev. B* **1988**, *37*, 785.

(59) Perdew, J. P.; Burke, K.; Ernzerhof, M. *Phys. Rev. Lett.* **1996**, *77*, 3865.

(60) Adamo, C.; Barone, V. *Chem. Phys. Lett.* **1998**, *298*, 113.

(61) Adamo, C.; Barone, V. *J. Chem. Phys.* **1999**, *110*, 6158.

(62) Zhao, Y.; Truhlar, D. G. *Theor. Chem. Acc.* **2008**, *120*, 215.

(63) Zhao, Y.; Truhlar, D. G. *J. Phys. Chem. A* **2008**, *110*, 13126.

(64) Grimme, S. *J. Chem. Phys.* **2006**, *124*, 034108.

(65) Karton, A.; Tarnopolsky, A.; Lamere, J. F.; Schatz, G. C.; Martin, J. M. L. *J. Phys. Chem. A* **2008**, *112*, 12868.

(66) Grimme, S. *J. Comput. Chem.* **2004**, *25*, 1463.

(67) Grimme, S. *J. Comput. Chem.* **2006**, *27*, 1787.

(68) Schwabe, T.; Grimme, S. *Acc. Chem. Res.* **2008**, *41*, 569.

(69) Korth, M.; Grimme, S. *J. Chem. Theory Comput.* **2009**, *5*, 993.

(70) Gruzman, D.; Karton, A.; Martin, J. M. L. *J. Phys. Chem. A* **2009**, *113*, 11974.

(71) Snook, I. K.; Per, M. C.; Seyed-Razavi, A.; Russo, S. P. *Chem. Phys. Lett.* **2009**, *480*, 327.

(72) Steinmann, S. N.; Csonka, G.; Corminboeuf, C. *J. Chem. Theory Comput.* **2009**, *5*, 2950.

(73) Zhao, Y.; Ng, H. T.; Hanson, E. *J. Chem. Theory Comput.* **2009**, *5*, 2726.

(74) Flener-Lovitt, C.; Woon, D. E.; Dunning, T. H., Jr.; Girolami, G. S. *J. Phys. Chem. A* **2010**, *114*, 1843.

(75) Marom, N.; Tkatchenko, A.; Scheffler, M.; Kronik, L. *J. Chem. Theory Comput.* **2010**, *6*, 81.

(76) Shamov, G. A.; Budzelaar, P. H. M.; Schreckenbach, G. *J. Chem. Theory Comput.* **2010**, *6*, 477.

(77) Boys, S. F.; Bernardi, F. *Mol. Phys.* **1970**, *19*, 553.

(78) Xantheas, S. S. *J. Chem. Phys.* **1996**, *104*, 8821.

(79) Szalewicz, K.; Jeziorski, B. *J. Chem. Phys.* **1998**, *109*, 1198.

(80) Varandas, A. J. C. *Theor. Chem. Acc.* **2008**, *119*, 511.

(81) Varandas, A. J. C. DOI:10.1021/jp908835v.

(82) Johnson, B. G.; Gonzales, C. A.; Will, P. M. W.; Pople, J. A. *Chem. Phys. Lett.* **1994**, *221*, 100.

(83) Porezag, D.; Pederson, M. R. *J. Chem. Phys.* **1995**, *102*, 9345.

(84) Csonka, G. I.; Johnson, B. G. *Theor. Chem. Acc.* **1998**, *99*, 158.

(85) Galano, A.; Alvarez-Idaboy, J. R.; Montero, L. A.; Vivier-Bunge, A. *J. Comput. Chem.* **2001**, *22*, 1138.

(86) Plesničar, B.; Tuttle, T.; Cerkovnik, J.; Koller, J.; Cremer, D. *J. Am. Chem. Soc.* **2003**, *125*, 11553.

(87) Wu, A.; Cremer, D.; Plesničar, B. *J. Am. Chem. Soc.* **2003**, *125*, 9395.

(88) Gräfenstein, J.; Kraka, E.; Cremer, D. *Phys. Chem. Chem. Phys.* **2004**, *6*, 1096.

(89) Tarnopolsky, A.; Karton, A.; Sertchook, R.; Vuzman, D.; Martin, J. M. L. *J. Phys. Chem. A* **2008**, *112*, 3.

(90) Lynch, B. J.; Truhlar, D. G. *J. Phys. Chem. A* **2001**, *105*, 2936.

(91) Zhao, Y.; González-Garcia, N.; Truhlar, D. G. *J. Phys. Chem. A* **2005**, *109*, 2012.

(92) Su, J. T.; Xu, X.; Goddard III, W. A. *J. Phys. Chem. A* **2004**, *108*, 10518.

(93) Halkier, A.; Klopper, W.; Helgaker, T.; Jørgensen, P.; Taylor, P. R. *J. Chem. Phys.* **1999**, *111*, 9157.

(94) Lin, R. J.; Wu, C. C.; Jang, S.; Li, F.-Y. *J. Mol. Model.* **2010**, *16*, 175.

(95) Pu, J.; Truhlar, D. G. *J. Chem. Phys.* **2002**, *116*, 1468.

(96) Jeanvoine, Y.; Spezia, R. *J. Mol. Struct.: THEOCHEM* **2010**, *954*, 7.

(97) Staroverov, V. N.; Scuseria, G. E.; Tao, J.; Perdew, J. P. *J. Chem. Phys.* **2003**, *119*, 12129.

(98) Lynch, B. J.; Fast, P. L.; Harris, M.; Truhlar, D. G. *J. Phys. Chem. A* **2000**, *104*, 4811.

(99) Zhao, Y.; Lynch, B. J.; Truhlar, D. G. *J. Phys. Chem. A* **2004**, *108*, 2715.

(100) Adamo, C.; Barone, V. *J. Chem. Phys.* **1998**, *108*, 664.

(101) Braams, B. J.; Yu, H.-G. *Phys. Chem. Chem. Phys.* **2008**, *10*, 3150.

(102) Dupuis, M.; Fitzgerald, G.; Hammond, B.; Lester, W. A., Jr.; Schaefer III, H. F. *J. Chem. Phys.* **1986**, *84*, 2691.

(103) Jungkamp, T. P. W.; Steinfeld, J. H. *Chem. Phys. Lett.* **1996**, *257*, 15.

(104) Suma, K.; Sumiyoshi, Y.; Endo, Y. *Science* **2005**, *308*, 1885.

(105) Mansergas, A.; Anglada, J. M.; Olivella, S.; Ruiz-López, M. F.; Martins-Costa, M. *Phys. Chem. Chem. Phys.* **2007**, *9*, 5865.

(106) Varner, M. E.; Harding, M. E.; Gauss, J.; Stanton, J. F. *Chem. Phys. Lett.* **2008**, *346*, 53.

(107) Wheeler, S. E.; Houk, K. N. *J. Chem. Theory Comput.* **2010**, *6*, 395.

CT100364X